INTERNATIONAL JOURNAL FOR NUMERICAL METHODS IN FLUIDS
Int. J. Numer. Meth. Fluids 2004; **45**:463–484 (DOI: 10.1002/fld.705)

A boundary-domain integral equation method in viscous fluid flow

Xiao-Wei Gao*,†

ZONA Technology, 7430 E. Stetson Drive, Scottsdale, AZ 85251, U.S.A.

SUMMARY

In this paper, the reciprocal work theorem for viscous fluid flow is established for Newtonian fluids and, based on this theorem, a set of boundary-domain integral equations is derived from the continuity and momentum equations for two-dimensional viscous flows. The complex-variable technique is used to compute velocity gradients in the use of the continuity equation. The primary variables involved in these integral equations are velocity, traction and pressure. Although the numerical implementation is only focused on steady incompressible flows, these equations are applicable to solving steady, unsteady, compressible and incompressible problems. In this method, the pressure can be expressed in terms of velocity and traction such that the final system of equations entering the iteration procedure only involves velocity and traction as unknowns. Two commonly cited numerical examples are presented to validate the derived equations. Copyright © 2004 John Wiley & Sons, Ltd.

KEY WORDS: viscous flow; continuity equation; Navier–Stokes equations; boundary integral method (BEM); domain integral

1. INTRODUCTION

The central governing equations in viscous flow are the Navier–Stokes (NS) equations (the momentum equations). Owing to the non-linearity of the convective terms appearing in the NS equations, only a few simple problems have analytical solutions [1]. For problems with complicated geometry or boundary conditions, numerical methods must be employed. The finite difference (FDM) [2], finite volume (FVM) [3] and finite element methods (FEM) [4] are well-established numerical methods for solving viscous flow problems. Among the three methods, FDM was first developed and is very simple to use although it requires very regular mesh [5]. In FEM, the penalty formulation is extensively used [6], but the determination of the penalty parameter is still controversial. The common feature of the three methods is that they are based on domain variable representations and local interpolation schemes, resulting in systems of equations that are highly spared matrices. Therefore, it is possible to use many nodes to discretize the domain of a problem. However, since the information

*Correspondence to: Xiao-Wei Gao, ZONA Technology, 7430 E. Stetson Drive, Scottsdale, AZ 85251, U.S.A.
†E-mail: gao@zonatech.com

Published online 8 April 2004

Received 5 May 2003
Revised 31 August 2003

is locally communicated by adjacent nodes, the computational accuracy is not as high as using the integral equation methods based on fundamental solutions. Moreover, since these methods rely on field information, it is impossible to develop a meshless algorithm to solve viscous flow problems. On the other hand, more and more references show that the boundary element method (BEM) is a promising technique for achieving this purpose by using the dual reciprocity method [7] or, more effectively, the radial integration method [8].

BEM is the most elegant numerical method for dealing with linear problems such as potential flows, linear elasticity and viscous creeping flows (Stokes equations). The most attractive feature of BEM is that the resulting system of equations only involve boundary quantities and their derivatives as unknowns. Therefore, only the boundary of the problem needs to be discretized into elements. Unfortunately, this distinct advantage is lost in solving non-linear problems such as the Navier–Stokes equations. For non-linear problems, domain integrals inevitably appear in the boundary integral equations. As a result, the non-linear region of the domain needs to be discretized into internal cells in order to evaluate the domain integral. Nevertheless, if the non-linear region is not large, BEM is still an efficient numerical tool. Apart from this, BEM is very robust in solving aerodynamics problems since the boundary conditions at infinity are automatically satisfied.

The first integral equation analysis for NS equations in terms of vorticity and velocity was carried out by Wu *et al.* in 1973 [9] through partitioning the mass and momentum conservation equations into kinematic and kinetic parts. The vorticity is determined by the non-linear transport equations, whereas the velocity is solved by an integral equation based on the fundamental solutions of the Laplace equation. Similar good works were conducted by Skerget *et al.* [10] and Onishi *et al.* [11] using the vorticity-stream function integral approach. The drawback of this type of technique is that the boundary conditions are not easy to set up in terms of vorticity and that the extension to three dimensions is not attractive.

In order to use the successfully established BEM theory in linear elasticity, Kitagawa *et al.* [12] and Grigoriev and Fafurin [13] utilized the penalty function method to solve incompressible flow problems based on the fundamental solutions of the Navier equation in elasticity by employing adequately large penalty parameters. Although nice results were obtained with this technique, using arbitrary penalty parameters results in an artificial compressibility of the flow.

A very elegant boundary integral equation can be obtained for incompressible flow by using the Stokeslet fundamental solutions [14]. The beauty of this technique is that the pressure is not included in the integral equations due to the use of the Stokeslet fundamental solutions which automatically satisfy the continuity equation. The first boundary element treatment using the Stokeslet fundamental solutions is attributed to the work by Bush and Tanner in 1983 [15] in which the local cell interpolation scheme is used to evaluate the velocity gradients. A similar idea appears in the recent work by Aydin and Fenner [16] with the difference being that the convective terms are treated using different finite difference schemes in different flow regions. To avoid the calculation of velocity gradients, Tosaka and Onishi [17] integrated the domain integrals by parts to remove the velocity gradients. This idea was further used by Tosaka and Fukushima [18] and Dargush and Banerjee [19]. The difference between the Dargush and Banerjee's work and others is that a different set of fundamental solutions is used and derived integral equations can account for thermal force effect in viscous flows. In order to evade the discretization of the domain into cells, Power and Partridge [20] transformed the domain integrals of the convective terms into boundary integrals by employing

the dual reciprocity method initiated by Nardini and Brebbia [7]. Further improvement to this technique refers to the works by Sarler and Kuhn [21], Power and Mingo [22] and Florez *et al.* [23].

Although the use of the Stokeslet fundamental solutions can result in velocity-traction only integral equations, the resulting BEM formulation is valid only for incompressible fluid flow. For compressible flow, such as in aerodynamics [5, 24], a new powerful integral formulation needs to be developed for general viscous flows. This paper is an attempt of the first step for this purpose.

In this paper, a reciprocal work theorem is first established from the constitutive relationship between stresses and strain rates. Then, based on this theorem, a set of velocity-traction-pressure integral equations is derived from the continuity equation and the momentum equations. The derived integral equations are valid for steady, unsteady, compressible and incompressible flows, although numerical implementation is only devoted to steady incompressible flows. The attractive feature of this method is that the pressure can be eliminated from the final system of equations. Consequently, the final iterative system is only related to the boundary unknowns (velocities or tractions) and internal velocities. In order to avoid evaluating strongly singular domain integrals, the complex-variable technique introduced to BEM by Gao *et al.* [25] is adopted to accurately evaluate the velocity gradients which are needed in the continuity equation. Finally, two commonly used examples, Couette flow and driven cavity flow, will be used to validate the formulation derived in this paper.

2. GOVERNING EQUATIONS OF VISCOUS FLOW

The governing equations in fluid mechanics can be derived from the conservation laws of mass, momentum and energy [26]. In this paper, the flow is assumed to be under isothermal condition, so conservation of energy is not concerned. The primitive equations are given in an inertial system and using Cartesian co-ordinates. The conservation of mass results in the following *continuity* equation:

$$\frac{\partial \rho}{\partial t} + \frac{\partial \rho u_i}{\partial x_i} = 0 \quad \text{or} \quad \frac{\partial \rho}{\partial t} + (\rho u_i)_{,i} = 0 \tag{1}$$

where t is time, ρ the fluid density and u_i the ith velocity component. The repeated subscript stands for summation and $()_{,i} = \partial()/\partial x_i$. For incompressible flow, the above equation reduces to $u_{i,i} = 0$.

The conservation of momentum (Newton's second law) can be expressed as

$$\sigma_{ij,j} + \rho b_i = \rho \frac{\partial u_i}{\partial t} + \rho u_j u_{i,j} \tag{2}$$

where b_i is the body force per unit mass (e.g. the gravity force) and σ_{ij} the stress tensor. For Newtonian fluid, the constitutive relationship between the stresses and strain rates can be expressed based on Stokes' hypothesis as

$$\sigma_{ij} = -p\delta_{ij} + 2\mu(\varepsilon_{ij} - \delta_{ij}\varepsilon_{kk}/3) \tag{3}$$

in which p is the pressure, δ_{ij} the Kronecker delta function, μ the viscosity (constant) and ε_{ij} the rate of strain tensor given by

$$\varepsilon_{ij} = (u_{i,j} + u_{j,i})/2 \tag{4}$$

Equations (3) and (4) show that both σ_{ij} and ε_{ij} are symmetric tensors. On substituting Equation (4) into (3) and the result into Equation (2), one can obtain the well-known Navier–Stokes equations.

On the fluid surface with outward normal n_i, the relationship between the stress and the traction t_i (force per unit area) can be expressed as

$$t_i = \sigma_{ij} n_j \tag{5}$$

Based on these equations, a new and powerful boundary integral equation set can be derived. To do this, the reciprocal work theorem for the viscous fluid flow needs to be established.

3. THE RECIPROCAL WORK THEOREM FOR VISCOUS FLUID FLOW

Apart from the set of quantities appearing in the previous section, we consider another set of velocity, pressure, stress and strain rates which satisfies Equations (1)–(5) and is denoted by an asterisk. Thus, according to Equation (3), we have

$$\sigma_{ij} + p\delta_{ij} = 2\mu(\varepsilon_{ij} - \delta_{ij}\varepsilon_{kk}/3) \tag{6}$$

$$\sigma^*_{ij} + p^*\delta_{ij} = 2\mu(\varepsilon^*_{ij} - \delta_{ij}\varepsilon^*_{kk}/3) \tag{7}$$

Multiplying both sides of Equation (6) by ε^*_{ij} and (7) by ε_{ij}, it follows that

$$(\sigma_{ij} + p\delta_{ij})\varepsilon^*_{ij} = 2\mu(\varepsilon_{ij}\varepsilon^*_{ij} - \varepsilon^*_{ii}\varepsilon_{kk}/3) \tag{8}$$

$$(\sigma^*_{ij} + p^*\delta_{ij})\varepsilon_{ij} = 2\mu(\varepsilon^*_{ij}\varepsilon_{ij} - \varepsilon_{ii}\varepsilon^*_{kk}/3) \tag{9}$$

Since $\varepsilon_{kk} = \varepsilon_{ii}$ and $\varepsilon^*_{kk} = \varepsilon^*_{ii}$, Equations (8) and (9) give

$$(\sigma_{ij} + p\delta_{ij})\varepsilon^*_{ij} = (\sigma^*_{ij} + p^*\delta_{ij})\varepsilon_{ij} \tag{10}$$

Consequently, the following integral statement holds true:

$$\int_\Omega (\sigma_{ij} + p\delta_{ij})\varepsilon^*_{ij}\,\mathrm{d}\Omega = \int_\Omega (\sigma^*_{ij} + p^*\delta_{ij})\varepsilon_{ij}\,\mathrm{d}\Omega \tag{11}$$

where Ω is the domain of the problem.

Equation (11) is the reciprocal work theorem for viscous flow. It implies that the work done by the stress set of the first system on the strain rates of the second system is equal to the work done by the stress set of the second system on the strain rates of the first system.

4. INTEGRAL EQUATIONS FOR VISCOUS FLUID FLOWS

4.1. General integral equation

Using relationship (4), the left-hand side of Equation (11) can be integrated by parts as

$$I_{\mathrm{L}} = \int_{\Omega} (\sigma_{ij} + p\delta_{ij})\varepsilon^*_{ij}\,\mathrm{d}\Omega = \int_{\Omega} \sigma_{ij} u^*_{i,j}\,\mathrm{d}\Omega + \int_{\Omega} p\delta_{ij} u^*_{i,j}\,\mathrm{d}\Omega$$
$$= \int_{\Gamma} \sigma_{ij} n_j u^*_i\,\mathrm{d}\Gamma - \int_{\Omega} \sigma_{ij,j} u^*_i\,\mathrm{d}\Omega + \int_{\Omega} p\delta_{ij} u^*_{i,j}\,\mathrm{d}\Omega \tag{12}$$

where Γ is the boundary of Ω.

Similarly, the right-hand side of Equation (11) results in

$$I_{\mathrm{R}} = \int_{\Omega} (\sigma^*_{ij} + p^*\delta_{ij})\varepsilon_{ij}\,\mathrm{d}\Omega = \int_{\Gamma} \sigma^*_{ij} n_j u_i\,\mathrm{d}\Gamma - \int_{\Omega} \sigma^*_{ij,j} u_i\,\mathrm{d}\Omega + \int_{\Omega} p^*\delta_{ij} u_{i,j}\,\mathrm{d}\Omega \tag{13}$$

Integrating the last integral in Equation (13) by parts yields

$$\int_{\Omega} p^*\delta_{ij} u_{i,j}\,\mathrm{d}\Omega = \int_{\Gamma} p^*\delta_{ij} n_j u_i\,\mathrm{d}\Gamma - \int_{\Omega} p^*_{,j}\delta_{ij} u_i\,\mathrm{d}\Omega \tag{14}$$

Substituting Equation (14) into (13), it follows that

$$I_{\mathrm{R}} = \int_{\Gamma} (\sigma^*_{ij} + p^*\delta_{ij}) n_j u_i\,\mathrm{d}\Gamma - \int_{\Omega} (\sigma^*_{ij} + p^*\delta_{ij})_{,j} u_i\,\mathrm{d}\Omega \tag{15}$$

Let $I_{\mathrm{L}} = I_{\mathrm{R}}$ and use Equation (5) to yield

$$\int_{\Gamma} t_i u^*_i\,\mathrm{d}\Gamma - \int_{\Omega} \sigma_{ij,j} u^*_i\,\mathrm{d}\Omega + \int_{\Omega} p\delta_{ij} u^*_{i,j}\,\mathrm{d}\Omega = \int_{\Gamma} t^*_i u_i\,\mathrm{d}\Gamma - \int_{\Omega} (\sigma^*_{ij} + p^*\delta_{ij})_{,j} u_i\,\mathrm{d}\Omega \tag{16}$$

where

$$t^*_i = (\sigma^*_{ij} + p^*\delta_{ij}) n_j \tag{17}$$

The last integral in Equation (16) can be further reduced by choosing the (*) set to be the fundamental solutions of the following equations:

$$(\sigma^{j*}_{ik} + p^{j*}\delta_{ik})_{,k} + \delta(y - x)\delta_{ij} = 0 \tag{18}$$

where $\delta(y-x)$ is the Dirac delta function of y at point x. The Dirac delta function $\delta(y-x)$, sometimes referred to as an impulse function, is used to represent a quantity that has a point singularity (infinity at $y = x$) but is zero everywhere else. A very useful property of the Dirac delta function is that it can isolate the value of a continuous function $f(y)$ at a specific point x [27]; thus,

$$\int_{\Omega_x} f(y)\delta(y - x)\,\mathrm{d}y = f(x) \tag{19}$$

where Ω_x is a range of any-size that includes the point x.

In terms of Equations (3) and (4), Equation (18) can also be written as

$$\mu\left(u^*_{ij,kk} + \tfrac{1}{3}\, u^*_{kj,ki}\right) + \delta(y-x)\delta_{ij} = 0 \tag{20}$$

Now after substituting Equation (18) into the last integral in Equation (16) and accounting for Equation (19), replacing u_i^* with the fundamental solution $u^*_{ij}(x, y)$ and t_i^* with the corresponding term $t^*_{ij}(x, y)$, we obtain

$$u_i(x) = \int_\Gamma u^*_{ij}(x, y) t_j(y)\, \mathrm{d}\Gamma(y) - \int_\Gamma t^*_{ij}(x, y) u_j(y)\, \mathrm{d}\Gamma(y) + \int_\Omega u^*_{ij,j}(x, y)\, p(y)\, \mathrm{d}\Omega(y) - \int_\Omega u^*_{ij}(x, y)\sigma_{jk,k}(y)\, \mathrm{d}\Omega(y) \tag{21}$$

Eliminating the term $\sigma_{jk,k}$ in Equation (21) using Equation (2), we can obtain the boundary integral equations involving the convective term $u_j u_{i,j}$ which may be treated as the 'pseudo-body force' as done by Bush and Tanner [15] and Power and Mingo [22]. However, this strategy results in a slow iterative convergence in solving the system of equations. In this paper, the velocity gradient involved in the convective term is eliminated in the following way. Using the continuity equation (1), the momentum equation (2) can be written as

$$\sigma_{jk,k}(y) = \frac{\partial \rho(y) u_j(y)}{\partial t} - \rho(y) b_j(y) + (\rho u_j u_k)_{,k} \tag{22}$$

Substituting this equation into Equation (21), it follows that

$$u_i(x) = \int_\Gamma u^*_{ij}(x, y) t_j(y)\, \mathrm{d}\Gamma(y) - \int_\Gamma t^*_{ij}(x, y) u_j(y)\, \mathrm{d}\Gamma(y) + \int_\Omega u^*_{ij,j}(x, y)\, p(y)\, \mathrm{d}\Omega(y) + \int_\Omega u^*_{ij}(x, y)\rho(y) b_j(y)\, \mathrm{d}\Omega(y) - \int_\Omega u^*_{ij}(x, y)\, \frac{\partial \rho(y) u_j(y)}{\partial t}\, \mathrm{d}\Omega(y) - \int_\Omega u^*_{ij}(x, y)(\rho u_j u_k)_{,k}\, \mathrm{d}\Omega(y) \tag{23}$$

As will be shown, the function $u^*_{ij}(x, y)$ has a singularity at the point $y = x$. However, since it is only a weakly singular integral, the last integral in the above equation can still be integrated by parts (see Appendix A). Consequently, the following boundary-domain integral equation can be obtained

$$u_i(x) = \int_\Gamma u^*_{ij}(x, y) t_j(y)\, \mathrm{d}\Gamma(y) - \int_\Gamma t^*_{ij}(x, y) u_j(y)\, \mathrm{d}\Gamma(y) - \int_\Gamma u^*_{ij}(x, y) n_k(y)\rho(y) u_j(y) u_k(y)\, \mathrm{d}\Gamma(y) + \int_\Omega u^*_{ij,k}(x, y)\rho(y) u_j(y) u_k(y)\, \mathrm{d}\Omega(y)$$

$$+\int_\Omega u_{ij}^*(x,y)\rho(y)b_j(y)\,\mathrm{d}\Omega(y)-\int_\Omega u_{ij}^*(x,y)\,\frac{\partial\rho(y)u_j(x)}{\partial t}\,\mathrm{d}\Omega(y)$$

$$+\int_\Omega u_{ij,j}^*(x,y)\,p(y)\,\mathrm{d}\Omega(y) \tag{24}$$

Equation (24) is a general boundary integral equation valid for steady, unsteady, compressible and incompressible flows. It also holds true for both 2D and 3D problems.

4.2. *Fundamental solutions for two-dimensional flows*

In 2D problems, the fundamental solutions of Equation (20) can be derived as

$$u_{ij}^*(x,y)=\frac{1}{16\pi\mu}\left\{7\delta_{ij}\ln\left(\frac{1}{r}\right)+r_{,i}\,r_{,j}\right\} \tag{25}$$

where r is the distance between points x and y, and

$$r_{,i}=\frac{y_i-x_i}{r} \tag{26}$$

The fundamental solution for traction can be obtained from Equations (17), (7), (25) and a relationship between ε_{ij}^* and u_i^* similar to Equation (4) as

$$t_{ij}^*(x,y)=\frac{-1}{8\pi r}\{3(n_i r_{,j}-n_j r_{,i})+(2r_{,i}\,r_{,j}+3\delta_{ij})n_k r_{,k}\} \tag{27}$$

Other used quantities can be derived by directly differentiating Equation (25) as

$$u_{ij,k}^*(x,y)=\frac{-1}{16\pi\mu r}\{7\delta_{ij}r_{,k}-\delta_{ik}r_{,j}-\delta_{jk}r_{,i}+2r_{,i}\,r_{,j}\,r_{,k}\} \tag{28}$$

$$u_{ij,j}^*(x,y)=\frac{-3r_{,i}}{8\pi\mu r} \tag{29}$$

Equations (25)–(29) show that these fundamental solutions have a singularity at the point $y=x$, therefore all integrals in Equation (24) should be interpreted in the Cauchy principal value sense. From the kernel function $t_{ij}^*(x,y)$ in Equation (27), we can see that the second integral in Equation (24) is strongly singular when the source point (collocation point) x approaches the field point y. Therefore, Equation (24) is only bounded for internal collocation points. Fortunately, the rigid body motion strategy can be used to handle this integral for boundary collocation points. The procedure is exactly the same as in the conventional BEM [27]. It is not repeated here. Except for the second integral, all other integrals in Equation (24) are weakly singular and therefore can be evaluated accurately by using the element/cell sub-division technique [27].

In Equation (24), pressure p appears in the domain integral and therefore one more equation is needed for this unknown. In addition, the velocity/traction-pressure coupled equation set may result from Equation (24). In the next section, one more equation will be provided based on the continuity equation and the pressure will be separated from the velocity/traction equation set.

5. INTEGRAL EQUATIONS BASED ON CONTINUITY EQUATION

The continuity equation (1) can be written as

$$\frac{\partial \rho}{\partial t} + u_i \frac{\partial \rho}{\partial x_i} + \rho \frac{\partial u_i}{\partial x_i} = 0 \tag{30}$$

In order to use this equation, the divergence of velocity needs to be determined. To do this, differentiating Equation (24) with respect to the source point x yields

$$\begin{aligned}\frac{\partial u_i(x)}{\partial x_i} = & \int_\Gamma \frac{\partial u_{ij}^*(x,y)}{\partial x_i} t_j(y)\,\mathrm{d}\Gamma(y) - \int_\Gamma \frac{\partial t_{ij}^*(x,y)}{\partial x_i} u_j(y)\,\mathrm{d}\Gamma(y) \\ & - \int_\Gamma \frac{\partial u_{ij}^*(x,y)}{\partial x_i} n_k(y)\rho(y)u_j(y)u_k(y)\,\mathrm{d}\Gamma(y) \\ & + \int_\Omega \frac{\partial u_{ij,k}^*(x,y)}{\partial x_i} \rho(y)u_j(y)u_k(y)\,\mathrm{d}\Omega(y) \\ & + \int_\Omega \frac{\partial u_{ij}^*(x,y)}{\partial x_i} \rho(y)b_j(y)\,\mathrm{d}\Omega(y) - \int_\Omega \frac{\partial u_{ij}^*(x,y)}{\partial x_i} \frac{\partial \rho(y)u_j(y)}{\partial t}\,\mathrm{d}\Omega(y) \\ & + \int_\Omega \frac{\partial u_{ij,j}^*(x,y)}{\partial x_i} p(y)\,\mathrm{d}\Omega(y)\end{aligned} \tag{31}$$

All integrals in the above equation need to be evaluated accurately in the Cauchy principal value sense. However, the direct differentiation of kernels makes the singularities one order higher. Especially, the kernel $\partial u_{ij,k}^*(x,y)/\partial x_i$ will become strongly singular. To avoid the direct differentiation, the complex-variable method (CVM) introduced in the BEM by Gao *et al.* [25] is adopted to evaluate the derivatives of all kernels appearing in Equation (31). Using CVM, the order of singularity can be reduced by one. Before doing this, let us first evaluate the domain integral including the pressure p.

5.1. Integration of domain integral involving pressure

The domain integral involving the pressure p in Equation (31) can be analytically integrated. Cutting a small circular domain Ω_ε with radius ε centred at point x from domain Ω (Figure 1) and noticing that $\partial()/\partial x_i = -\partial()/\partial y_i = -()_{,i}$ for solution (25), we have

$$\begin{aligned}\int_\Omega \frac{\partial u_{ij,j}^*(x,y)}{\partial x_i} p(y)\,\mathrm{d}\Omega(y) &= -\lim_{\varepsilon\to 0}\int_{\Omega-\Omega_\varepsilon} u_{ij,ji}^*(x,y)p(y)\,\mathrm{d}\Omega(y) - p(x)\lim_{\varepsilon\to 0}\int_{\Omega_\varepsilon} \frac{\partial u_{ij,j}^*(x,y)}{\partial y_i}\,\mathrm{d}\Omega(y) \\ &= -\int_\Omega u_{ij,ji}^*(x,y)p(y)\,\mathrm{d}\Omega(y) - p(x)\lim_{\varepsilon\to 0}\int_{\Gamma_\varepsilon} u_{ij,j}^*(x,y)n_i\,\mathrm{d}\Gamma(y)\end{aligned}$$

where Γ_ε is the boundary of the circular domain Ω_ε. By differentiating Equation (29), one can find that $u_{ij,ji}^*(x,y) = 0$. So the first integral in the right-hand side of the above equation

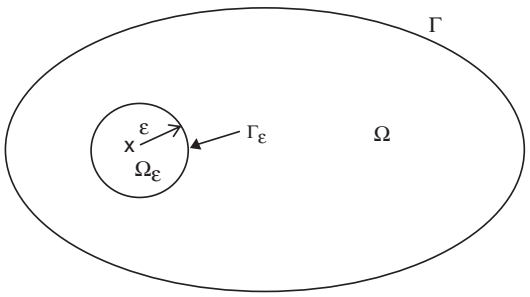

Figure 1. A small domain Ω_ε cut out from Ω.

disappears and the second one can be easily integrated as

$$\int_\Omega \frac{\partial u^*_{ij,j}(x,y)}{\partial x_i}\, p(y)\, \mathrm{d}\Omega(y) = \frac{3}{4\mu}\, p(x) \tag{32}$$

5.2. Evaluation of derivatives of singular kernels using complex-variable method

In CVM, the variable x of a real function $f(x)$ is replaced by a complex one, $x + Ih$. For a very small h, $f(x + Ih)$ can be expanded into a Taylor's series as follows:

$$f(x + Ih) = f(x) + Ih\, \frac{\mathrm{d}f}{\mathrm{d}x} + \cdots$$

Thus, the derivative of the above equation can be expressed as

$$\frac{\mathrm{d}f}{\mathrm{d}x} = \frac{\mathrm{Im}(f(x + Ih))}{h} \tag{33}$$

where the symbols 'Im' denotes the imaginary part. From Equation (33), it can be seen that the derivative using the complex variable approach only requires function evaluation. This feature is very attractive particularly when the function is sufficiently complicated. Unlike in the finite difference method, no cancellation errors exist in CVM. In numerical implementation, the step-size h is usually set to 10^{-20}, so that the result is step-size independent. CVM can be easily used to evaluate the derivatives appearing in Equation (31). Let us consider the co-ordinates at the source point x as complex variables by adding a small imaginary part Ih to the ith co-ordinate. According to Equation (33) and accounting for Equation (32), if follows from Equation (31) that

$$\begin{aligned}\frac{\partial u_i(x)}{\partial x_i} = &\int_\Gamma u'^*_j(x,y) t_j(y)\, \mathrm{d}\Gamma(y) - \int_\Gamma t'^*_j(x,y) u_j(y)\, \mathrm{d}\Gamma(y) \\ &- \int_\Gamma u'^*_j(x,y) n_k(y) \rho(y) u_j(y) u_k(y)\, \mathrm{d}\Gamma(y) \\ &+ \int_\Omega u'^*_{j,k}(x,y) \rho(y) u_j(y) u_k(y)\, \mathrm{d}\Omega(y)\end{aligned}$$

$$+\int_\Omega u_j'^*(x,y)\rho(y)b_j(y)\,\mathrm{d}\Omega(y)-\int_\Omega u_j'^*(x,y)\,\frac{\partial \rho u_j}{\partial t}\,\mathrm{d}\Omega(y)$$
$$+\frac{3}{4\mu}\,p(x) \tag{34}$$

where

$$u_j'^*(x,y)=\frac{1}{h}\,\mathrm{Im}(u_{ij}^*(x_i+Ih,y))$$
$$t_j'^*(x,y)=\frac{1}{h}\,\mathrm{Im}(t_{ij}^*(x_i+Ih,y)) \tag{35}$$
$$u_{j,k}'^*(x,y)=\frac{1}{h}\,\mathrm{Im}(u_{ij,k}^*(x_i+Ih,y))$$

Comparison of Equation (34) with Equation (24) reveals that the singularities involved in the expression of divergence of the velocity are the same as occurred in the velocity integral equation (24) and are only weakly singular. Therefore, every integral in Equation (34) can be evaluated accurately for internal points. For boundary points, the kernel t_{ij}^* is still singular even using CVM, so the traction-recovery method is used in this paper. The implement procedure of the traction-recovery method is similar to the computation of the boundary stresses in the convention BEM. Readers may refer to Reference [27] for details.

Substituting Equation (34) into (30), we can obtain the desired integral equation to close the equation set provided by Equations (24) for problems with velocities/tractions and pressures as unknowns. Using Equations (34) and (30), the pressure can be expressed in terms of velocities and tractions. Therefore, the final system of equations only includes velocities/tractions as unknowns. For compressive flows, the density ρ is also unknown. In this case, the energy equation and equation of state are required to close the final system of equations and the unknowns will be velocity/traction, density and temperature. This will be described in a future work.

6. NUMERICAL IMPLEMENTATION FOR STEADY INCOMPRESSIBLE FLOWS

In this section, the detailed numerical implementation of Equations (24) and (34) in steady incompressible flows is described. In this case, the density ρ is constant and the time-related domain integrals in Equations (24) and (34) disappear. Thus, the continuity equation (30) becomes

$$\frac{\partial u_i}{\partial x_i}=0 \tag{36}$$

6.1. Algebraic system of equations

Numerical implementation of Equations (24) and (34) requires discretization of the boundary Γ into boundary elements and the domain Ω into internal cells. For each boundary element or internal cell, the velocity, traction and pressure can be expressed in terms of their nodal values through shape functions as follows:

$$u_j=\sum_\alpha N_\alpha u_j^\alpha \tag{37}$$

$$t_j = \sum_{\alpha} N_\alpha t_j^\alpha \tag{38}$$

$$p = \sum_{\alpha} N_\alpha p^\alpha \tag{39}$$

where N_α are shape functions for boundary elements and internal cells [27], u_j^α represents the value of u_j at node α. Usually, the non-linear term $u_j u_k$ is formed by Equation (37). However, for the sake of simplicity to assemble, the following linearized formulation is used:

$$u_j u_k = \sum_{\alpha} N_\alpha u_j^\alpha u_k^\alpha \tag{40}$$

This approximation enables us to assemble the coefficient matrices node by node.

Substituting Equations (37)–(40) into the discretized form of the integral equation (24) and collocating x for all boundary nodes (rigid body motion is used for determination of diagonal terms) yields the following algebraic matrix equation:

$$[H]\{u\} = [G]\{t\} + \{b\} + [C_b]\{p\} + [D_b]\{u^2\} \tag{41}$$

where $\{u\}$ and $\{t\}$ are vectors consisting of velocities and tractions at all boundary nodes, respectively, and $\{b\}$ is constant vector from body forces. And $\{p\}$ and $\{u^2\}$ are vectors consisting of pressure and velocity products at all nodes (i.e. boundary and internal nodes). The latter can be clearly shown as

$$\{u^2\} = \{(u_1^1)^2, u_1^1 u_2^1, (u_2^1)^2, (u_1^2)^2, u_1^2 u_2^2, (u_2^2)^2, \ldots, (u_1^n)^2, u_1^n u_2^n, (u_2^n)^2\}^{\mathrm{T}} \tag{42}$$

in which n is the total number of all nodes.

In each direction of a boundary node, either velocity or traction is specified as a boundary condition. So after applying the boundary conditions to Equation (41) and rearrange the equation, it follows that

$$[A_b]\{X\} = \{Y_b\} + [C_b]\{p\} + [D_b]\{u^2\} \tag{43}$$

where $\{X\}$ is a vector consisting of unknown velocities and unknown tractions, and $\{Y_b\}$ is a known vector. Similarly, for internal nodes, Equation (24) gives

$$\{u_I\} = [A_I]\{X\} + \{Y_I\} + [C_I]\{p\} + [D_I]\{u^2\} \tag{44}$$

where $\{u_I\}$ is the vector consisting of all velocities at internal nodes. Finally, substituting Equation (34) into (36) yields

$$\{p\} = [A_p]\{X\} + \{Y_p\} + [D_p]\{u^2\} \tag{45}$$

Since for boundary nodes, the traction-recovery method [27] can also result in an equation similar to Equation (45), we assume that Equation (45) represents the equations for both boundary and internal nodes.

Now substituting Equation (45) into (43), we can obtain

$$\{X\} = \{Y^x\} + [D^x]\{u^2\} \tag{46}$$

where

$$\begin{aligned}\{Y^x\} &= [A]^{-1}(\{Y_b\} + [C_b]\{Y_p\}) \\ \{D^x\} &= [A]^{-1}([D_b] + [C_b][D_p])\end{aligned} \tag{47}$$

here

$$[A] = [A_b] - [C_b][A_p] \tag{48}$$

Then substituting Equation (46) into (45) yields

$$\{p\} = \{Y^p\} + [D^p]\{u^2\} \tag{49}$$

where

$$\begin{aligned}\{Y^p\} &= \{Y_p\} + [A_p]\{Y^x\} \\ [D^p] &= [D_p] + [A_p][D^x]\end{aligned} \tag{50}$$

Finally, substituting Equations (46) and (49) into (44), we obtain the matrix equations for internal velocities

$$\{u^I\} = \{Y^I\} + [D^I]\{u^2\} \tag{51}$$

where

$$\begin{aligned}\{Y^I\} &= \{Y_I\} + [A_I]\{Y^x\} + [C_I]\{Y^p\} \\ [D^I] &= [D_I] + [A_I][D^x] + [C_I][D^p]\end{aligned} \tag{52}$$

Equations (46), (49) and (51) constitute the final system of equations with $\{X\}$ and $\{u^I\}$ as unknowns. Since they are non-linear equations about velocities, an iterative procedure is required to solve them. Among the three equations, only Equations (46) and (51) are used in the iterative process. Once the iteration converges, the values of velocities are plugged in Equation (49) to compute the pressures. The advantage of the equation set presented above over the existing "pseudo-body force" representations is that the velocities explicitly appear in the system of equations. Therefore, the first and second derivatives of the system with respect to velocities can be easily derived so that any advanced non-linear equation solver can be applied to solve the system of equations. In the following section, the Newton–Raphson scheme is described in detail.

6.2. Solving system of equations using the Newton–Raphson scheme

The notation $\{X\}_i$ and $\{u^I\}_i$ is used to denote the boundary unknowns and internal velocities, respectively, after the ith iteration. The residuals of Equations (46) and (51), following the ith iteration, can be written as

$$\begin{aligned}\{R^x\}_i &= \{Y^x\}_i + [D^x]\{u^2\}_i - \{X\}_i \\ \{R^I\}_i &= \{Y^I\}_i + [D^I]\{u^2\}_i - \{u^I\}_i\end{aligned} \tag{53}$$

Our objective is to reduce the residual to zero. If we force $\{R^x\}_{i+1}$ and $\{R^I\}_{i+1}$ to be zero, we obtain

$$0 = \{R^x\}_{i+1} = \{R^x\}_i + \frac{\partial\{R^x\}_i}{\partial\{X\}_i}\{\Delta X\} + \frac{\partial\{R^x\}_i}{\partial\{u^I\}_i}\{\Delta u^I\} \tag{54}$$

$$0 = \{R^I\}_{i+1} = \{R^I\}_i + \frac{\partial\{R^I\}_i}{\partial\{X\}_i}\{\Delta X\} + \frac{\partial\{R^I\}_i}{\partial\{u^I\}_i}\{\Delta u^I\} \tag{55}$$

where $\{\Delta X\}$ and $\{\Delta u^I\}$ are the changes in the boundary unknowns and internal velocities. Combining Equations (54) and (55) yields

$$\begin{bmatrix} \dfrac{\partial\{R^x\}_i}{\partial\{X\}_i} & \dfrac{\partial\{R^x\}_i}{\partial\{u^I\}_i} \\ \dfrac{\partial\{R^I\}_i}{\partial\{X\}_i} & \dfrac{\partial\{R^I\}_i}{\partial\{u^I\}_i} \end{bmatrix} \begin{Bmatrix} \{\Delta X\} \\ \{\Delta u^I\} \end{Bmatrix} = - \begin{Bmatrix} \{R^x\}_i \\ \{R^I\}_i \end{Bmatrix} \tag{56}$$

where

$$\begin{aligned} \frac{\partial\{R^x\}_i}{\partial\{X\}_i} &= [D^x][UX] - [I] \\ \frac{\partial\{R^x\}_i}{\partial\{u^I\}_i} &= [D^x][UI] \\ \frac{\partial\{R^I\}_i}{\partial\{X\}_i} &= [D^I][UX] \\ \frac{\partial\{R^I\}_i}{\partial\{u^I\}_i} &= [D^I][UI] - [I] \end{aligned} \tag{57}$$

in which, $[I]$ is the identity matrix, and $[UX]$ and $[UI]$ are formed by the derivatives of $\{u^2\}$ with respect to boundary unknown velocities and internal velocities, respectively, i.e.

$$[UX] = \begin{bmatrix} [U_x'^1] & 0 & \cdots & 0 \\ 0 & [U_x'^2] & \cdots & 0 \\ \vdots & \vdots & & \vdots \\ 0 & 0 & \cdots & [U_x'^{n_b}] \\ 0 & 0 & \cdots & 0 \\ \vdots & \vdots & & \vdots \\ 0 & 0 & \cdots & 0 \end{bmatrix} \tag{58}$$

$$[UI] = \begin{bmatrix} 0 & 0 & \cdots & 0 \\ \vdots & \vdots & \vdots & \\ [U_I'^{n_b+1}] & 0 & \cdots & 0 \\ 0 & [U_I'^{n_b+2}] & \cdots & 0 \\ \vdots & \vdots & & \vdots \\ 0 & 0 & \cdots & [U_I'^{n}] \end{bmatrix} \tag{59}$$

where n_b and n are the numbers of boundary nodes and total nodes, respectively, and for node k

$$[U_x'^k] = \begin{bmatrix} 2u_1^k\lambda_1 & 0 \\ u_2^k\lambda_1 & u_1^k\lambda_2 \\ 0 & 2u_2^k\lambda_2 \end{bmatrix} \tag{60}$$

$$[U_I'^k] = \begin{bmatrix} 2u_1^k & 0 \\ u_2^k & u_1^k \\ 0 & 2u_2^k \end{bmatrix} \tag{61}$$

In Equation (60), $\lambda_1 = 0$ if the velocity is specified in the x-direction at node k, otherwise $\lambda_1 = 1$. The same rule is applied to λ_2, but for the y-direction.

Solving Equation (56) for $\{\Delta X\}$ and $\{\Delta u^I\}$, the values of unknowns are updated using the equations

$$\begin{aligned} \{X\}_{i+1} &= \{X\}_i + \{\Delta X\} \\ \{u^I\}_{i+1} &= \{u^I\}_i + \{\Delta u^I\} \end{aligned} \tag{62}$$

With these new values, we go back to Equation (53) to do the next iteration. Once convergence is achieved, that is, the norm of $\{R^x\}_i$ and $\{R^I\}_i$ is less than a specified tolerance, the pressure can be computed using Equation (45).

It is noted that in the iteration, only matrices $[U_x'^k]$ and $[U_I'^k]$ need to be recomputed. Other matrices are formed only once and can be stored on a disk for subsequent iteration use.

7. NUMERICAL EXAMPLES

Two numerical examples of two-dimensional steady incompressible viscous flows are presented in this section to demonstrate the correctness of the results derived in this paper. The first one is the well-known Couette flow which has analytical solutions to verify and the second one is the driven cavity flow for which the benchmark solution is available [28]. These two examples were computed on a PC computer (2 GHz, 256 Mb RAM).

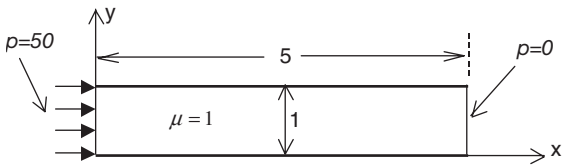

Figure 2. Geometry and boundary condition for Couette flow.

Table I. Horizontal velocities along y-direction.

y	0.125	0.25	0.375	0.5	0.625	0.75	0.875
Current	0.54609	0.9363	1.17033	1.2484	1.170331	0.9362	0.546081
Exact	0.54687	0.9375	1.17187	1.25	1.171875	0.9375	0.546875

7.1. *Couette flow*

In order to validate the formulations derived in this paper, the simplest Couette flow is considered first. The flow is two dimensional, between two flat plates without body forces (Figure 2).

The 'no-slip' condition is applied to the upper and lower sides. Mathematically, the boundary conditions can be expressed as

$$\left.\begin{aligned} t_x &= p = 50 \\ u_y &= 0 \end{aligned}\right\} \quad \text{on side } x = 0$$

$$\left.\begin{aligned} t_x &= p = 0 \\ u_y &= 0 \end{aligned}\right\} \quad \text{on side } x = 5$$

$$\left.\begin{aligned} u_x &= 0 \\ u_y &= 0 \end{aligned}\right\} \quad \text{on sides } y = 0 \text{ and } y = 1$$

For this simple problem, analytical solutions are available [29]. The horizontal velocity can be expressed as

$$u_x = -\frac{p'}{2\mu}\, y(H - y)$$

where $H = 1$ is the distance between upper and lower sides, $p' = \mathrm{d}p/\mathrm{d}x = 10$ is the gradient of pressure.

For the BEM model, both upper and lower sides are discretized into 40 equally spaced linear boundary elements and left and right sides into 18 elements. Totally, there are 112 boundary elements and 112 boundary nodes. The domain is discretized into 640 equally sized internal cells with 585 internal nodes. Table I lists the computed horizontal velocities and analytical solutions along y-direction at $x = 2.5$. Figure 3 is a plot of the velocity profile. Although this problem is density independent, in order to examine the convergence of iteration, the

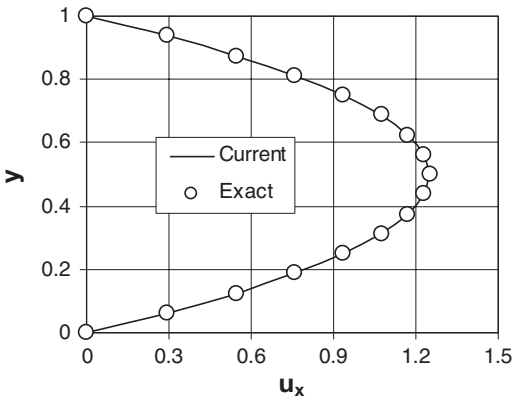

Figure 3. Velocity profile on vertical lines.

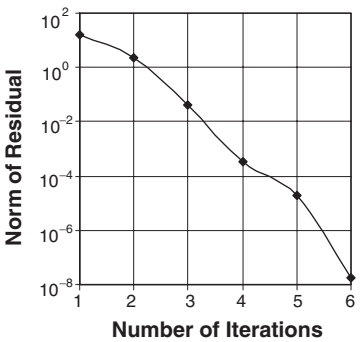

Figure 4. Iteration history for Couette flow.

computation is carried out by setting the density ρ to 1. Figure 4 shows the convergence history of iteration for a convergence tolerance of 10^{-8}. The computational time spent for this example is 45 s.

From Figure 3, we can see that the results from the current method are in good agreement with the exact solutions and Figure 4 shows that very rapid convergence can be achieved for this simple example.

7.2. Driven flow in a unitary square cavity

The second numerical example concerned is a unitary square cavity (Figure 5). The top wall moves with a uniform velocity of 1 in the horizontal direction, while the other walls are fixed including two corners of the top side. Ghia *et al.* [28] presented a benchmark solution that is commonly cited for comparison purposes (e.g. Reference [16]). Each wall is discretized into 80 equally spaced linear boundary elements with a total of 160 elements and 160 nodes around the cavity. The domain of the cavity is approximated with 1600 linear quadrilateral cells with 1521 internal nodes.

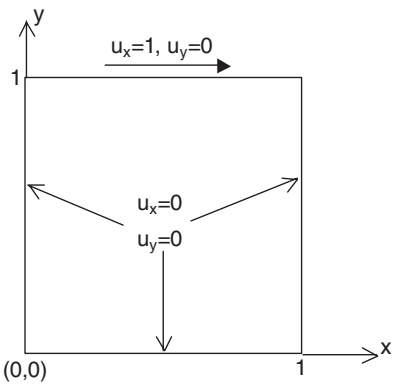

Figure 5. Geometry and boundary conditions for driven cavity flow.

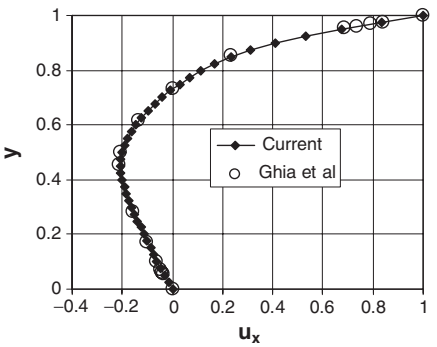

Figure 6. Horizontal velocity profile on vertical centre line of the driven cavity.

The Reynolds number is defined as $Re = \rho UH/\mu$, where U is the characteristic velocity and H the characteristic length. In this example, the parameters are set as $\rho = 100$, $U = 1$, $H = 1$, and $\mu = 1$. This implies that $Re = 100$. Figure 6 shows the computed horizontal velocities on vertical centre line of the cavity and Figure 7 depicts the vertical velocity profile on the horizontal centre line. The traction distribution over the top of the cavity is plotted in Figure 8. The traction singularity at corners of the cavity can be clearly revealed in Figure 8. In order to have a global sight of the flow in the cavity, Figure 9 gives the velocity vector plot. The computed vortex centre location is (0.6153, 0.7354), which is close to the result (0.6172, 0.7344) by Ghia *et al.* [28]. The iteration history is shown in Figure 10 for the given convergence tolerance of 10^{-10}. The convergence is achieved after 29 iterations. The computational time spent for this example is 17 min.

Comparison of the current results with the benchmark solutions in Figures 6 and 7 indicates that the method described in this paper is correct and the iteration history in Figure 10 shows that fast convergence can be achieved using the current method.

In this example, the computational results are given only for the case of Reynolds number $Re = 100$. More computations with higher Reynolds numbers were also conducted using

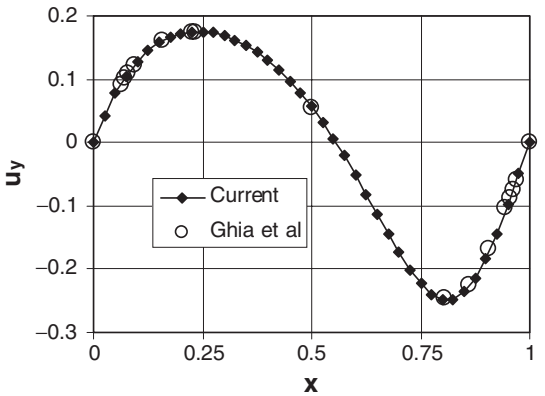

Figure 7. Vertical velocity profile on horizontal centre line of the driven cavity.

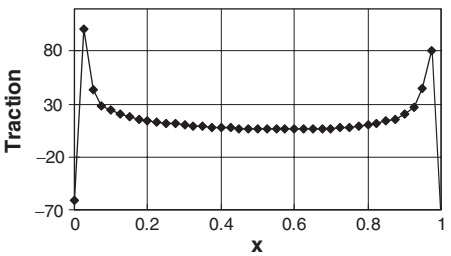

Figure 8. Traction distribution along top wall.

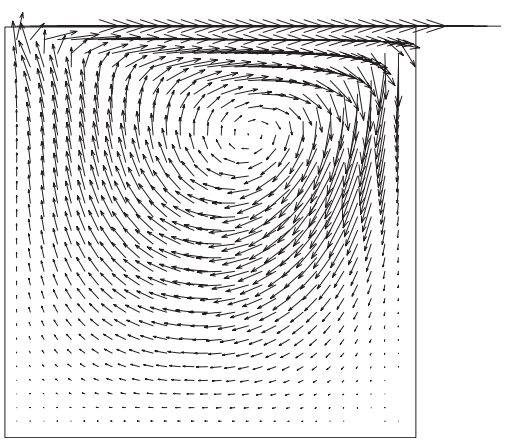

Figure 9. Velocity vectors.

the same computational model. Good convergence can only be achieved for Reynolds number $Re \leqslant 220$. This may be the limit of using the basic Newton–Raphson iteration scheme. For higher Reynolds number cases, an advanced non-linear equation solver [30–32] may be

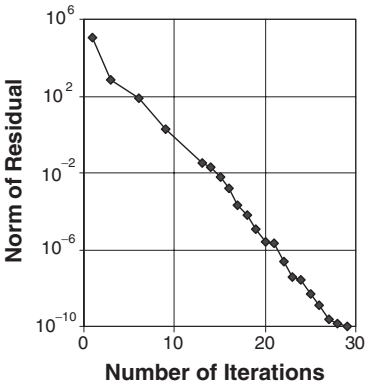

Figure 10. Iteration history for driven cavity flow.

necessary or finer boundary elements and internal cells may be required. However, this has exceeded our currently available resources.

8. CONCLUDING REMARKS

A new boundary-domain integral equation method is presented for viscous fluid flow problems, for which a complete set of fundamental solutions is given for two-dimensional problems. The derived formulation is general and promising, applicable to steady, unsteady, compressible and incompressible flows. Two numerical results for steady incompressible flows demonstrated the correctness of the method.

Although the pressure is included in the basic integral equation (Equation (24)), decoupled system of equations can be achieved by using the continuity equation to eliminate the pressure term. This is a beneficial feature of the BEM as compared to other numerical methods for solving viscous flow problems. This feature enables us to reduce unknowns by one for each node to save computer memory and computational time.

Owing to the use of the complex-variable technique to compute the divergence of velocity, no strongly singular domain integrals need to be treated particularly and therefore accurate results can be obtained.

The distinct advantage of the presented formulation is that velocities explicitly appear in the system of equations (without including velocity gradients). Therefore, the existing powerful non-linear system solvers can be easily employed to solve the system of equations.

In this paper, only the basic Newton–Raphson scheme is described in solving the non-linear system. Acceleration technique, such as the relaxation technique [16, 30] can be applied to improve the convergence speed and stability of the Newton–Raphson scheme. Alternatively, one can also use advanced non-linear solvers, such as the modified Powell hybrid algorithm with Jacobian [31]. To save storage, the use of the variable metric method in multi-dimensions is effective [32]. Using this method, the derivative (Jacobian) matrix needs not to be inverted directly.

APPENDIX A

To treat the last integral in Equation (23), we divide the integral domain Ω into two parts, $\Omega - \Omega_\varepsilon$ and Ω_ε, with Ω_ε being an infinitesimal circular range with radius ε and centred at point x (see Figure 1). Thus,

$$\int_\Omega u_{ij}^*(x,y)(\rho u_j u_k)_{,k}\,\mathrm{d}\Omega(y) = \lim_{\varepsilon\to 0}\int_{\Omega-\Omega_\varepsilon} u_{ij}^*(x,y)(\rho u_j u_k)_{,k}\,\mathrm{d}\Omega(y) + \lim_{\varepsilon\to 0}\int_{\Omega_\varepsilon} u_{ij}^*(x,y)(\rho u_j u_k)_{,k}\,\mathrm{d}\Omega(y) \tag{A1}$$

where the fundamental solution u_{ij}^* is determined by Equation (25).

Let us consider a polar co-ordinate system (r,θ) with the origin at the centre of the circle Γ_ε. In this system, the quantity $r_{,i}$ is a function of θ only (see Equation (26)). Assuming that the velocity is continuous, the last integral in Equation (A1) can be operated as

$$\begin{aligned}\lim_{\varepsilon\to 0}\int_{\Omega_\varepsilon} u_{ij}^*(x,y)(\rho u_j u_k)_{,k}\,\mathrm{d}\Omega(y) &= (\rho u_j u_k)_{,k}|_{y=x}\lim_{\varepsilon\to 0}\int_0^{2\pi}\int_0^{\varepsilon} u_{ij}^*(x,y) r\,\mathrm{d}r\,\mathrm{d}\theta\\ &= (\rho u_j u_k)_{,k}|_{y=x}\frac{1}{64\pi\mu}\int_0^{2\pi}\left(\lim_{\varepsilon\to 0}\varepsilon^2[7(1-2\ln\varepsilon)\delta_{ij}+2r_{,i}r_{,j}]\right)\mathrm{d}\theta\\ &= (\rho u_j u_k)_{,k}|_{y=x}\frac{1}{64\pi\mu}\int_0^{2\pi} 0\,\mathrm{d}\theta = 0\end{aligned} \tag{A2}$$

The first integral on the right-hand side of Equation (A1) is regular since the point x is located outside the domain $\Omega - \Omega_\varepsilon$ which is bounded by boundaries Γ and Γ_ε. Thus, integrating this integral by parts yields

$$\begin{aligned}\lim_{\varepsilon\to 0}\int_{\Omega-\Omega_\varepsilon} u_{ij}^*(x,y)(\rho u_j u_k)_{,k}\,\mathrm{d}\Omega(y) &= \int_\Gamma u_{ij}^*(x,y)n_k(y)\rho(y)u_j(y)u_k(y)\,\mathrm{d}\Gamma(y)\\ &\quad+\lim_{\varepsilon\to 0}\int_{\Gamma_\varepsilon} u_{ij}^*(x,y)n_k(y)\rho(y)u_j(y)u_k(y)\,\mathrm{d}\Gamma(y)\\ &\quad-\lim_{\varepsilon\to 0}\int_{\Omega-\Omega_\varepsilon} u_{ij,k}^*(x,y)\rho(y)u_j(y)u_k(y)\,\mathrm{d}\Omega(y)\\ &= \int_\Gamma u_{ij}^*(x,y)n_k(y)\rho(y)u_j(y)u_k(y)\,\mathrm{d}\Gamma(y)\\ &\quad-\int_\Omega u_{ij,k}^*(x,y)\rho(y)u_j(y)u_k(y)\,\mathrm{d}\Omega(y)\\ &\quad+\rho(x)u_j(x)u_k(x)\lim_{\varepsilon\to 0}\int_{\Gamma_\varepsilon} u_{ij}^*(x,y)n_k(y)\,\mathrm{d}\Gamma(y)\end{aligned} \tag{A3}$$

Since the boundary Γ_ε is a circle and the outward normal n_k in the last integral of Equation (A3) is directed inward, it follows that $n_k = -r_{,k}$. Thus, noticing that $r = \varepsilon$ and $r_{,k}$ is a function of θ only, we have

$$\lim_{\varepsilon\to 0}\int_{\Gamma_\varepsilon} u^*_{ij}(x,y)n_k\,\mathrm{d}\Gamma(y) = -\lim_{\varepsilon\to 0}\int_0^{2\pi} u^*_{ij}(x,y)r_{,k}r\,\mathrm{d}\theta$$

$$= -\int_0^{2\pi}\left[\lim_{\varepsilon\to 0}\varepsilon u^*_{ij}(x,y)\right]r_{,k}\,\mathrm{d}\theta \tag{A4}$$

From Equation (25) we can see that the function $u^*_{ij}(x,y)$ is a weakly singular function, so that

$$\lim_{\varepsilon\to 0}\varepsilon u^*_{ij}(x,y) = 0 \tag{A5}$$

Finally, combining Equations (A1)–(A5), we obtain

$$\int_\Omega u^*_{ij}(x,y)(\rho u_j u_k)_{,k}\,\mathrm{d}\Omega(y) = \int_\Gamma u^*_{ij}(x,y)n_k(y)\rho(y)u_j(y)u_k(y)\,\mathrm{d}\Gamma(y)$$

$$-\int_\Omega u^*_{ij,k}(x,y)\rho(y)u_j(y)u_k(y)\,\mathrm{d}\Omega(y) \tag{A6}$$

REFERENCES

1. Bourchtein A. Exact solutions of the generalized Navier–Stokes equations for benchmarking. *International Journal for Numerical Methods in Fluids* 2002; **39**:1053–1071.
2. Roache PJ. *Computational Fluid Dynamics* (revised edn). Hermosa Press: Albuquerque, 1976.
3. Patankar SV. *Numerical Heat Transfer and Fluid Flow*. McGraw-Hill: New York, 1980.
4. Reddy JN, Gartling DK. *The Finite Element Method in Heat Transfer and Fluid Dynamics*. CRC Press: Boca Raton, FL, 1987.
5. Gao XW, Chen PC, Tang L. Deforming mesh for computational aeroelasticity using a nonlinear elastic boundary element method. *AIAA Journal* 2002; **40**:1512–1517.
6. Eguchi Y. A new positive-definite regularization of incompressible Navier–Stokes equations discretized with Q1/P0 finite element. *International Journal for Numerical Methods in Fluids* 2003; **41**:881–904.
7. Nardini D, Brebbia CA. A new approach for free vibration analysis using boundary elements. In *Boundary Element Methods in Engineering*, Brebbia CA (ed.). Springer: Berlin, 1982; 312–326.
8. Gao XW. The radial integration method for evaluation of domain integrals with boundary-only discretization. *Engineering Analysis with Boundary Elements* 2002; **26**:905–916.
9. Wu JC, Thompson JF. Numerical solutions of time-dependent incompressible Navier–Stokes equations using an integral-differential formulation. *Computers in Fluids* 1973; **1**:197–215.
10. Skerget P, Alujevic A, Brebbia CA. The solution of Navier–Stokes equations in terms of vorticity-velocity variables by boundary elements. In *BEM VI*. Computational Mechanics Publications: Southampton, 1984.
11. Onishi K, Kuroki T, Tanaka M. An application of the boundary element method to incompressible laminar viscous flow. *Engineering Analysis* 1984; **1**:122–127.
12. Kitagawa K, Brebbia CA, Wrobel LC, Tanaka M. Boundary element analysis of viscous flow by penalty function formulation. *Engineering Analysis* 1986; **3**:194–200.
13. Grigoriev MM, Fafurin AV. A boundary element method for steady viscous fluid flow using penalty function formulation. *International Journal for Numerical Methods in Fluids* 1997; **25**:907–929.
14. Ladyzhenskaya OA. *The Mathematical Theory of Viscous Incompressible Flow*. Gordon and Breach: New York, 1963.
15. Bush MB, Tanner RI. Numerical solution of viscous flows using integral equation method. *International Journal for Numerical Methods in Fluids* 1983; **3**:71–92.

16. Aydin M, Fenner RT. Boundary element analysis of driven cavity flow for low and moderate Reynolds numbers. *International Journal for Numerical Methods in Fluids* 2001; **37**:45–64.
17. Tosaka N, Onishi K. Boundary integral equations formulations for steady Navier–Stokes equations using the Stokes fundamental solution. *Engineering Analysis with BEM* 1985; **2**:128–132.
18. Tosaka N, Fukushima N. Integral equation analysis of laminar natural convection problems. In *BEM VIII*. Computational Mechanics Publications: Southampton, Springer: Berlin, 1986.
19. Dargush GF, Banerjee PK. A boundary element method for steady incompressible thermoviscous flow. *International Journal for Numerical Methods in Engineering* 1991; **31**:1605–1626.
20. Power H, Partridge PW. The use of Stokes' fundamental solution for the boundary only formulation of the three-dimensional Navier–Stokes equations for moderate Reynolds numbers. *International Journal for Numerical Methods in Engineering* 1994; **37**:1825–1840.
21. Sarler B, Kuhn G. Primitive variable dual reciprocity boundary element method solution of incompressible Navier–Stokes equations. *Engineering Analysis with Boundary Elements* 1999; **23**:443–455.
22. Power H, Mingo R. The DRM subdomain decomposition approach to solve the two-dimensional Navier–Stokes system of equations. *Engineering Analysis with Boundary Elements* 2000; **24**:107–119.
23. Florez WF, Power H, Chejne F. Multi-domain dual reciprocity BEM approach for the Navier–Stokes system of equations. *Communications in Numerical Methods in Engineering* 2000; **16**:671–681.
24. Liu DD, Chen PC, Tang L, Chang KT, Gao XW. Expedient hypersonic aerothermodynamics methodology for RLV/TPS design. In *Proceedings of AIAA/AAAF 11th International Space Planes and Hypersonic Systems and Technologies Conference*, Orleans, France, 29 September–4 October 2002; 1–9.
25. Gao XW, Liu DD, Chen PC. Internal stresses in inelastic BEM using complex-variable differentiation. *Computational Mechanics* 2002; **28**:40–46.
26. White FM. *Viscous Fluid Flow* (2nd edn). McGraw-Hill: Boston, 1991.
27. Gao XW, Davies TG. *Boundary Element Programming in Mechanics*. Cambridge University Press: Cambridge, MA, 2002.
28. Ghia U, Ghia KN, Shin CT. High-Re solutions for incompressible flow using the Navier–Stokes equations and a multigrid method. *Journal of Computational Physics* 1982; **48**:387–411.
29. Granger RA. *Fluid Mechanics*. Dover: New York, 1995.
30. Florez WF. *Nonlinear Flow Using Dual Reciprocity*. WIT Press: Southampton, 2001.
31. More JB, Hillstrom K. *User guide for MINPACK-1*. Argonne National Labs Report ANL80-74, Argonne, IL, 1980.
32. Press WH, Flannery BP, Teukolsky SA, Vetterling WT. *Numerical Recipes*: *The Art of Scientific Computing*. Cambridge University Press: Cambridge, MA, 1986; 307–312.

